Clim. Past Discuss., https://doi.org/10.5194/cp-2018-80
Manuscript under review for journal Clim. Past
Discussion started: 17 July 2018

Climate of the Past Discussions

120,000 year record of sea ice in the North Atlantic

Niccolò Maffezzoli[1], Paul Vallelonga[1], Ross Edwards[2,3], Alfonso Saiz-Lopez[4], Clara Turetta[5,6], Helle Astrid Kjær[1], Carlo Barbante[5,6], Bo Vinther[1], and Andrea Spolaor[5,6]

[1]Centre for Ice and Climate, Niels Bohr Institute, University of Copenhagen, Juliane Maries Vej 30, Copenhagen Ø 2100, Denmark
[2]Physics and Astronomy, Curtin University of Technology, Kent St, Bentley, WA 6102, Perth, Australia
[3]Department of Civil and Environmental Engineering, UW-Madison, Madison, WI 53706, USA
[4]Department of Atmospheric Chemistry and Climate, Institute of Physical Chemistry Rocasolano, CSIC, Madrid, Spain
[5]Ca' Foscari University of Venice, Department of Environmental Sciences, Informatics and Statistics, Via Torino 155, 30170 Venice Mestre, Italy
[6]Institute for the Dynamics of Environmental Processes, IDPA-CNR, Via Torino 155, 30170 Venice Mestre, Italy

Correspondence: N. Maffezzoli (maffe@nbi.ku.dk)

Abstract. Although it has been demonstrated that the speed and magnitude of recent Arctic sea ice decline is unprecedented for the past 1,450 years, few records are available to provide a paleoclimate context for Arctic sea ice extent. Here we present a 120 kyr record of bromine enrichment from the RECAP ice core, coastal East Greenland, and reconstruct past sea ice conditions in the North Atlantic as far north as the entrance of the Arctic Ocean (50-85 °N). Bromine enrichment has been previously employed to reconstruct first-year sea ice (FYSI) in the Canadian Arctic over the last glacial cycle. We find that during the last deglaciation, the transition from multi-year sea ice (MYSI) to FYSI started at ∼17.6 kyr, synchronous with sea ice reductions observed in the eastern Nordic seas (Müller and Stein, 2014; Hoff et al., 2016) and with the increase of North Atlantic ocean temperature (Dokken and Jansen, 1999). FYSI reached its maximum extent at 12.4-11.8 kyr, after which open-water conditions started to dominate, as supported by sea ice records from the eastern Nordic seas and the North Icelandic shelf. Our results show that over the last 120,000 years, sea ice extent was greatest during Marine Isotope Stage (MIS) 2 and MIS4, with decreased levels during MIS3 and the onset of the last glacial period (late-MIS5). Sea ice extent during the last 10 kyr (Holocene/MIS1) has been less than at any time in the last 120 kyr.

1 Introduction

The connection between Arctic sea ice and bromine was first identified through an anticorrelation between springtime ground level ozone (O_3) and filterable bromine concentrations (Barrie et al., 1988). Large bromine oxide (BrO) column enhancements and simultaneous tropospheric ozone depletion were later found in Antarctica (Kreher et al., 1997). Satellite observations reveal geographically-widespread 'bromine explosions', the sudden increase of atmospheric bromine concentrations during springtime occurring in both polar regions (Chance, 1998; Richter et al., 1998; Wagner and Platt, 1998). The primary sources of reactive bromine in the polar atmosphere remained unclear until bromine recycling over fresh sea ice surfaces was suggested to occur at polar sunrise. The mechanism proceeds via springtime photochemical heterogeneous reactions over fresh sea ice surfaces that lead to activation of bromide, followed by the release and exponential increase of gas-phase bromine species in the

Clim. Past Discuss., https://doi.org/10.5194/cp-2018-80
Manuscript under review for journal Clim. Past
Discussion started: 17 July 2018

Climate of the Past Discussions

polar troposphere (Vogt et al., 1996). Several saline substrates on fresh sea ice surfaces were suggested as reservoir of reactive sea salt aerosol (SSA) capable of sustaining bromine recycling (Abbatt et al., 2012; Saiz-Lopez and von Glasow, 2012). To date, both model studies (Yang et al., 2008, 2010) and experimental evidence (Pratt et al., 2013; Zhao et al., 2016) consider the deposited snow layer on FYSI (known as salty blowing snow) to be the most efficient substrate for SSA release and bromine activation. Atmospheric bromine and sodium originate from both oceanic and FYSI sea salt aerosol, where they are found in mass ratios identical to that of sea water. As a consequence of bromine recycling on FYSI surfaces, the atmospheric bromine-to-sodium mass ratio is increased with respect to that of sea water, leading to a bromine enrichment ($\mathrm{Br_{enr}}$), observed in polar snow. Measurements of $\mathrm{Br_{enr}}$ in ice cores can thus be used to reconstruct FYSI conditions (Spolaor et al., 2014).

The first Arctic glacial-interglacial investigation of $\mathrm{Br_{enr}}$ was performed on the NEEM ice core, located in Northwest Greenland and representing sea ice aerosol from the Canadian archipelago, Baffin Bay and Hudson Bay (Spolaor et al., 2016). The NEEM 120 kyr sea ice reconstruction found greater $\mathrm{Br_{enr}}$ values during the Holocene and interstadials, pointing to greater FYSI conditions during such periods. Lower $\mathrm{Br_{enr}}$ values during colder climate phases indicated more extended multi-year sea ice (MYSI) coverage.

2 The RECAP ice core and the $\mathrm{Br_{enr}}$ record

Here, we investigate past sea ice conditions in the North Atlantic Ocean, based on the $\mathrm{Br_{enr}}$ record extracted from the RECAP ice core, located in coastal East Greenland. Because of its location, the record is sensitive to ocean processes and sea ice dynamics (Cuevas et al., 2018). We compare our sea ice record with $\mathrm{PIP_{25}}$ results from three marine sediment cores drilled within the Renland source area: the Fram Strait, the Norwegian Sea and the North Icelandic shelf. The $\mathrm{PIP_{25}}$ index is a semi-quantitative indicator of the local sea ice condition at the marine core location. It is calculated by coupling the sediment concentration of $\mathrm{IP_{25}}$, a biomarker produced by diatoms living in seasonal sea ice, with an open water phytoplankton biomarker (brassicasterol or dinosterol, hence $\mathrm{P_BIP_{25}}$ or $\mathrm{P_DIP_{25}}$). Briefly, the $\mathrm{PIP_{25}}$ index is a dimentionless number varying from 0 to 1: $\mathrm{PIP_{25}} \approx 1$ indicates perennial sea ice cover; $\mathrm{PIP_{25}} \approx 0$ indicates open water conditions, while intermediate $\mathrm{PIP_{25}}$ values reflect seasonal sea ice (Müller et al., 2011; Belt and Müller, 2013).

The RECAP ice core was drilled in 2015 in the Renland peninsula and covers the last 120,000 years (Appendix A). A back trajectory analysis spanning the 2000-2016 period indicates that Renland is associated with a different SSA source area compared to the NEEM ice core (Appendix B). The source of Renland SSA has been constrained to the ocean basin extending in latitude from 50° N to 85° N (corresponding to the North Atlantic up to the Fram Strait) and in longitude from the western coasts of Norway and the UK to East Greenland (Fig. B1). Thus Renland receives a negligible SSA contribution from West Greenland waters. The source region is nowadays mostly dominated by open water (OW) and FYSI conditions, with only minor contributions of MYSI, transported south from the Arctic Ocean alongside the East Greenland coastline via the Transpolar Drift.

Sodium and bromine concentrations were determined by Inductively Coupled Plasma Mass Spectroscopy (ICP-MS, Appendix A1). The bromine enrichment values, $\mathrm{Br_{enr}}$, were calculated according to the following equations:

Clim. Past Discuss., https://doi.org/10.5194/cp-2018-80
Manuscript under review for journal Clim. Past
Discussion started: 17 July 2018

Climate of the Past Discussions

$$\mathrm{Br_{enr}} = \frac{[Br]}{0.0062[ssNa]} \tag{1}$$

$$[ssNa] = \frac{[Cl]}{1.8} \longleftrightarrow \frac{[Cl]}{[Na]} < 1.8 \tag{2}$$

$$[ssNa] = [Na] \longleftrightarrow \frac{[Cl]}{[Na]} \geq 1.8 \tag{3}$$

where [Br] and [ssNa] are the bromine and sea-salt sodium concentrations in the ice samples, 1.8 and 0.0062 are respectively the chlorine/sodium and bromine/sodium sea water mass ratios (Millero et al., 2008).

Since sodium has a potential crustal contribution, which can be significant especially during arid periods (i.e. stadials), it was necessary to extract its marine contribution. For this purpose, we used chlorine, which was measured along with bromine and sodium by ICP-SFMS (Cl/Na record in Fig. 1). Chlorine/sodium mass ratios greater than that of seawater are observed in polar ice cores during warm climate periods due to acid-scavenged (HNO_3 and H_2SO_4) dechlorination of sea salt aerosols (e.g. $2NaCl + H_2SO_4 \rightarrow 2HCl + Na_2SO_4$). The removal of gas-phase HCl is believed to be more efficient during warmer climatic conditions, resulting in Cl/Na ratios beyond the sea water reference (Legrand and Delmas, 1988), since HCl has a longer atmospheric residence time than SSA. No correction to sodium is therefore applied when Cl/Na $\geq$ 1.8. The sodium crustal contribution was found to be up to 29% during 60-70 kyr and 15% at ∼23 kyr, consistent with the results from the Renland 1988 ice core (Hansson, 1994).

The $\mathrm{Br_{enr}}$ time series (Fig. 2) displays values greater than 1 throughout the record, suggesting a persistent FYSI influence. Values are on average low during the Holocene ($\mathrm{Br_{enr,Hol}}$ = 3.8, RMS(root mean square) = 1.4, MIS1) and during the coldest glacial phases, with glacial minima at ∼23 kyr ($\mathrm{Br_{enr,LGM}}$ = 3.2±0.2(1σ), MIS2) and at ∼72 kyr ($\mathrm{Br_{enr}}$ = 2.6±0.4(1σ), MIS4). At the Eemian termination, ∼120 kyr, $\mathrm{Br_{enr}}$ was slightly higher with respect to what is observed during the Holocene ($\mathrm{Br_{enr,120kyr}}$ = 4.9, RMS = 1.1, MIS5), suggesting that more FYSI was present in this period with respect to the mean Holocene value.

3 Results and discussion

In accordance with their respective SSA source regions, the Canadian Arctic sea ice reconstruction from the NEEM ice core (Spolaor et al., 2016) is markedly different from the North Atlantic sea ice record reconstructed here. In the NEEM core, $\mathrm{Br_{enr}}$ was positively correlated to $\delta^{18}O$ throughout the entire climatic record (Spolaor et al., 2016). In contrast, at Renland, such a consistent correlation is not present, and $\mathrm{Br_{enr}}$ is at times lower during warmer climate periods (e.g. during the Holocene). We suggest that this difference originates from the fact that during warm periods, while the NEEM site is influenced by FYSI in the Canadian Arctic, Baffin Bay and Hudson Bay, Renland faces mostly OW conditions in the North Atlantic. Since a lower $\mathrm{Br_{enr}}$ value indicates a reduced bromine activation from FYSI surfaces, low values of $\mathrm{Br_{enr}}$ can indicate either OW or MYSI conditions. Hence, at Renland, we suggest that the former occurs during the Holocene, while the latter occurred during the coldest parts of the glacial. $\mathrm{Br_{enr}}$ is therefore a signature, at Renland, of contrasting sea ice states: FYSI/MYSI and

Clim. Past Discuss., https://doi.org/10.5194/cp-2018-80
Manuscript under review for journal Clim. Past
Discussion started: 17 July 2018

Climate of the Past Discussions

FYSI/OW. In the framework of this dual regime behavior, a 'tipping point' is to be expected whenever there is a shift from one regime to the other (Fig. 4). One such shift occurs during the deglaciation. At the Last Glacial Maximum (LGM, ∼23 kyr), the low enrichment value ($\mathrm{Br_{enr,LGM}}$ = 3.2±0.2) suggests reduced FYSI recycling and therefore increased MYSI (increased OW conditions are considered very unlikely in this cold climatic phase). Moving from the Last Glacial Maximum into the Holocene, $\mathrm{Br_{enr}}$ increases until ∼12 kyr ($\mathrm{Br_{enr,12kyr}}$ = 7.5±0.5), indicating maximum FYSI at this time (Fig. 2 and Fig. 3). Hereafter, a decrease is observed, as $\mathrm{Br_{enr}}$ continues to drop during the Early Holocene (Fig. 2).

3.1 The last deglaciation

We now consider in further detail the last deglaciation, when a number ocean temperature, salinity and circulation modifications coincide with changes in Nordic seas and North Atlantic sea ice as reconstructed here. $\mathrm{PIP_{25}}$ records from both the Svalbard margin (eastern Fram Strait, from Müller and Stein 2014 and the Norwegian Sea, from Hoff et al. 2016) indicate (Fig. 3) that near-perennial sea ice ($\mathrm{PIP_{25}} \approx$ 0.5-1) was present during MIS 2 until ∼17 kyr (17.6 kyr recorded in the Svalbard margin), the onset of a major breakup of extensive sea ice cover, during Heinrich Event 1 (18 to 15 kyr). Synchronous to within a few centuries, several modifications relevant to the North Atlantic ocean are observed, including sea water surface freshening and warming in the polar and subpolar North Atlantic (a record from 67 °N, Dokken and Jansen 1999, is shown as an example in Fig. 3) and a near total cessation of the Atlantic Meridional Overturning Circulation (McManus et al., 2004). Generally low to intermediate $\mathrm{PIP_{25}}$ values ($\mathrm{PIP_{25}} \approx$ 0-0.5) are reported at the Fram Strait from this point until ∼12 kyr, with a slight increasing trend throughout the Bølling-Allerød (BA) and a broad maximum reached during the Younger Dryas (YD), suggesting that seasonal sea ice conditions were present in the ∼17-12 kyr period. Marine records in the eastern Nordic Seas also indicate milder sea ice conditions during the BA and increased sea ice during the YD (Belt et al., 2015; Cabedo-Sanz et al., 2016). In contrast, a record from the northern Icelandic Shelf (Xiao et al. 2017, Fig. 3) shows that sea ice conditions remained near-perennial from 14.7 to 11.7 kyr ($\mathrm{PIP_{25}} \approx$ 0.5-1). Xiao et al. suggest that this pattern of more severe sea ice conditions in the north of Iceland is, at least during the BA and the YD, linked to the flow of warmer waters from the North Atlantic Current, influencing sea ice melting in the eastern Nordic Seas, whereas the Icelandic shelf is influenced by colder polar waters from the East Greenland Current and the East Icelandic Current.

The RECAP ice core was resampled at sub-centennial resolution to better constrain the timing of sea ice changes through the deglaciation in the 50-85 °N North Atlantic sampling region. These data (Fig. 3, stars) indicate that FYSI (i.e. $\mathrm{Br_{enr}}$) started to increase in the North Atlantic, concurrent to a reduction of MYSI, at ∼17.5 kyr, synchronous with local $\mathrm{PIP_{25}}$ decrease in the Fram Strait and eastern Nordic Seas and in response to sea surface temperature warming in the North Atlantic. This suggests that North Atlantic sea ice changes occur in concert with temperature and circulation changes of the underlying waters. We note that this time period also coincides with the initiation of deglacial changes in mean ocean temperature, Antarctic temperatures and atmospheric $\mathrm{CO_2}$ concentrations toward interglacial values (Bereiter et al., 2018). The synchronicity between the warmings in the Nordic Seas and in Antarctica, already reported at the onset of Dansgaard-Oeschger events (Rasmussen et al., 2016), can be thus extended to the sea ice in the North Atlantic. North Atlantic FYSI increases throughout the BA (except for one point at 12.7-12.4 kyr at the onset of the YD) until a maximum at 12.4-11.8 kyr during the YD (Fig. 3). From the comparison

Clim. Past Discuss., https://doi.org/10.5194/cp-2018-80
Manuscript under review for journal Clim. Past
Discussion started: 17 July 2018

Climate of the Past Discussions

between the marine and ice core results, we infer that, during the 17-12 kyr period, the 50-85 °N-integrated North Atlantic sea ice changed from MYSI to FYSI. Local sea ice was also melting at ∼17 kyr, in the eastern Nordic Seas, influenced by the North Atlantic Current, while, at least from 14.7 to 11.7 kyr, sea ice was still near-perennial over the Icelandic shelf, as influenced by polar waters carried on the East Greenland Current.

Following its maximum value at 12.4-11.8 kyr, Br enr (i.e. FYSI) started to decrease (Fig. 3). We suggest that from this point-in-time, the $\mathrm{Br_{enr}}$ indicator now shifts to the FYSI/OW regime (Fig. 4), and therefore lower values indicate more extensive OW. A retreating FYSI scenario is also recorded in all three marine cores (decreasing $\mathrm{PIP_{25}}$ to ≈ 0-0.4 during the Early Holocene, Fig. 3), suggesting that OW conditions progressively developed in the whole North Atlantic.

3.2 Dual $\mathrm{Br_{enr}}$ regime and $\mathrm{Br_{enr}}$ transformation

Since $\mathrm{Br_{enr}}$ is an increasing function of FYSI, its decrease points to either OW or MYSI conditions (Fig. 4), following either the FYSI/OW or the FYSI/MYSI regimes. At any point in time, only one regime is considered to be in place, and we suggest that a temperature threshold is the discriminating variable setting the regime type. Since a change of regime is observed during the deglaciation, with maximum $\mathrm{Br_{enr}}$ (i.e. FYSI) at 11.8-12.4 kyr, we set the threshold to be the mean NGRIP temperature reconstructed for that period: $\mathrm{T_{NGRIP}}$=-44.6±0.9 (2σ) °C. The regime type (FYSI/MYSI or FYSI/OW, see Fig. 4) is determined according to such a temperature threshold. The regime type in each ice sample is represented by the color of the error bars in Fig. 5: blue for the FYSI/MYSI regime and red for the FYSI/OW regime.

We suggest a procedure to linearize the $\mathrm{Br_{enr}}$ indicator with respect to the two climate regimes. The method is again based on the observation that during the deglaciation, $\mathrm{Br_{enr}}$ reaches its maximum value (i.e. maximum FYSI) at 11.8-12.4 kyr: $\overline{\mathrm{Br_{enr}}}$ = 7.4±0.5 (1σ) (Fig. 2 and Fig. 3). We now introduce the transformed-$\mathrm{Br_{enr}}$ indicator, which compensates for the decrease from this maximum value due to increasing MYSI conditions (only in the FYSI/MYSI regime) with an increase of the same magnitude (Eq. 5). No transformation affects the ice samples in the FYSI/OW regime (Eq. 4).

$$\begin{cases} \mathrm{Br_{enr}} \longrightarrow \mathrm{Br_{enr}} \\ T > \mathrm{T_{NGRIP}}(12.4-11.8\mathrm{kyr}) = -44.6 \pm 0.9(2\sigma)^{\circ}\mathrm{C} \end{cases} \tag{4}$$

$$\begin{cases} \mathrm{Br_{enr}} \longrightarrow \overline{\mathrm{Br_{enr}}} + (\overline{\mathrm{Br_{enr}}} - \mathrm{Br_{enr}}) \\ T < \mathrm{T_{NGRIP}}(12.4-11.8\mathrm{kyr}) = -44.6 \pm 0.9(2\sigma)^{\circ}\mathrm{C} \end{cases} \tag{5}$$

Standard error propagation is carried out when transforming $\mathrm{Br_{enr}}$ in Eq. 5.

The transformed-$\mathrm{Br_{enr}}$ variable (Fig. 5, lower panels) is now to be interpreted as being linearly variable between OW and MYSI conditions, therefore providing an absolute index of sea ice extent within the Renland source area.

In order to test the sensitivity of the regime output on the threshold value, 4 scenarios are computed, using a ±1σ and a ±2σ value around the temperature threshold mean value: -44.6 °C (Fig. 5. Left: -2σ:top; +2σ:bottom. Right: -1σ:top; +1σ:bottom).

Clim. Past Discuss., https://doi.org/10.5194/cp-2018-80
Manuscript under review for journal Clim. Past
Discussion started: 17 July 2018

We note that for the simple 2-state model applied here, discontinuities could occur for adjacent samples integrating temperature values close to the temperature threshold. Only at a few time periods, however, is the regime discrimination significantly affected by the chosen threshold value (see them discussed in the following section). MIS1 and MIS5 are characterized by the 'warm' FYSI/OW regime, while the 'cold' FYSI/MYSI regime occurs during MIS2 and MIS4. MIS3 shows a mixture between the two $\mathrm{Br_{enr}}$ regimes.

3.3 The 120,000 year sea ice record

The two North Atlantic sea ice time series, calculated by applying the $\pm 2\sigma$ transformation (i.e. allowing for the biggest discrepancies), are shown in Fig. 6. It is worth noting that since the $\overline{\mathrm{Br_{enr}}}$ sample integrates 1500 years, these two records have been downscaled to 1500 years.

Some discrepancies between the two reconstructed sea ice records are found. The first one is at the 23.3-17.3 kyr (Last Glacial Maximum), with reduced sea ice predicted for the 'lower' temperature threshold (see also Fig. 5). The second one, at 35.3-33.8 kyr (integrating Greenland Stadial GS-7, and Greenland Interstadial GI-7), results in opposite sea ice scenarios. Finally, at 72.8-71.3 kyr (integrating GI-19.2 and GS-20), both scenarios indicate a decrease in sea ice but of slightly different magnitude. The output of the transformation is sensitive to the chosen temperature threshold, and therefore could result in anomalous sea ice states during those climate periods when the temperature was close to the threshold. If the $\pm 1\sigma$ transformations are considered (Fig. 5, right panels), the two predicted sea ice scenarios would still display a slight discrepancy during the LGM, and during GI-19.2 and GS-20, while a sea ice reduction would be predicted for both scenarios during 35.3-33.8 kyr, likely associated with a sea ice decrease that occurred during GI-7.

With the exception of the aforementioned discrepant time periods, both reconstructions show that, over the last 120 kyr, sea ice was greatest during MIS2 and MIS4, the two climate periods characterized by the coldest temperatures and reduced insolation (Fig. 6). Sea ice during MIS3 and MIS5 was less extensive than during MIS2/MIS4. In particular, sea ice at the onset of the last glacial period ($\sim$120 kyr) was slightly more extended than during the late Holocene (MIS1), characterized by the lowest sea ice levels of the entire 120 kyr record. These results agree with local sea ice conditions reported from the Norwegian Sea for the last 90 kyr (Hoff et al. 2016, Fig. 6). Dansgaard-Oeschger (DO) millennial-scale oscillations cannot be fully resolved since our procedure has been downscaled to 1500 year resolution, although the model does indicate a sea ice decrease during GI (glacial interstadial) 7, 19 and 20, while a sea ice increase is found during GS-25. The RECAP ice core was subject to considerable glaciological thinning in the section containing glacial ice, therefore the sampling resolution used here is insufficient to resolve all DO transitions. Nonetheless, sea ice variability on DO-timescales has been reported for the Canadian Arctic, and comparable resolution is offered by the forthcoming EastGRIP ice core, located in Northeast Greenland.

4 Conclusions and Outlook

We present a method to reconstruct past sea ice conditions in the 50-85 °N-integrated North Atlantic ocean for the last 120,000 years from sodium and bromine measurements in the RECAP ice core. Our reconstruction shows that, during the last deglacia-

tion, sea ice started its transformation from multi-year sea ice to first-year sea ice ∼17.6 kyr, probably triggered by increasing surface ocean water temperatures. The maximum first-year sea ice signature is found at 12.4-11.8 kyr, whereupon open ocean was the dominant condition during the Holocene (MIS1). Although the RECAP sea ice record does not extend back to the warmest period of MIS5, it does show that sea ice extent during the Holocene is lower than at any time in the past 120 kyr. Sea ice extent was maximum during MIS2 and MIS4. Intermediate conditions, if compared to MIS2/MIS4, were present during MIS3 and late-MIS5. Increased time resolution is needed to fully resolve Dansgaard-Oeschger oscillations. Our sea ice reconstruction provides the first ice core-based observation of sea ice in the 50-85° N-integrated North Atlantic, an area where ocean dynamics has profound global climatic implications. This record will provide critical constrains on past North Atlantic sea ice conditions to climate models, advancing the knowledge of Arctic climate science, its feedbacks and implications for the whole climate system.

Data availability. The RECAP ice core data will be made available on NOAA paleoclimate and PANGAEA online data archives.

Author contributions. P.V. and A.S. conceived the experiment. N.M., R.E., P.V., A.S, H.A.K and C.T. collected the samples and ran the experimental analyses. N.M. analyzed and interpreted the results; B.M.V proposed the $\mathrm{Br_{enr}}$ transformation. N.M. wrote the manuscript with inputs from all authors.

Competing interests. The authors declare no competing financial interests.

Acknowledgements. The RECAP ice coring effort was financed by the Danish Research Council through a Sapere Aude grant, the NSF through the Division of Polar Programs, the Alfred Wegener Institute, and the European Research Council under the European Community's Seventh Framework Programme (FP7/2007-2013) / ERC grant agreement 610055 through the Ice2Ice project and the Early Human Impact project (267696). This study has also received funding from the European Research Council Executive Agency under the European Union's Horizon 2020 Research and innovation programme (Project 'ERC-2016-COG 726349 CLIMAHAL'). We thank our colleagues from the Continuous Flow Analysis group at Centre for Ice and Climate (Copenhagen, Denmark) for helping in the sample collection. We thank Trevor Popp, Steffen Bo Hansen and the RECAP drilling group, Joel Pedro, Markus Jochum and Trond Dokken for discussions. We thank Zhao Meixun for sharing the Icelandic core data.

Clim. Past Discuss., https://doi.org/10.5194/cp-2018-80
Manuscript under review for journal Clim. Past
Discussion started: 17 July 2018

Climate of the Past Discussions
Open Access
EGU

References

Abbatt, J., Thomas, J. L., Abrahamsson, K., Boxe, C., Granfors, A., Jones, A., King, M., Saiz-Lopez, A., Shepson, P., Sodeau, J., et al.: Halogen activation via interactions with environmental ice and snow in the polar lower troposphere and other regions, Atmospheric Chemistry and Physics, 12, 6237–6271, 2012.

Barrie, L., Bottenheim, J., Schnell, R., Crutzen, P., and Rasmussen, R.: Ozone destruction and photochemical reactions at polar sunrise in the lower Arctic atmosphere, Nature, 334, 138–141, 1988.

Belt, S. T. and Müller, J.: The Arctic sea ice biomarker IP 25: a review of current understanding, recommendations for future research and applications in palaeo sea ice reconstructions, Quaternary Science Reviews, 79, 9–25, 2013.

Belt, S. T., Cabedo-Sanz, P., Smik, L., Navarro-Rodriguez, A., Berben, S. M., Knies, J., and Husum, K.: Identification of paleo Arctic winter sea ice limits and the marginal ice zone: optimised biomarker-based reconstructions of late Quaternary Arctic sea ice, Earth and Planetary Science Letters, 431, 127–139, 2015.

Bereiter, B., Shackleton, S., Baggenstos, D., Kawamura, K., and Severinghaus, J.: Mean global ocean temperatures during the last glacial transition, Nature, 553, 39, 2018.

Bigler, M., Svensson, A., Kettner, E., Vallelonga, P., Nielsen, M. E., and Steffensen, J. P.: Optimization of high-resolution continuous flow analysis for transient climate signals in ice cores, Environmental Science & Technology, 45, 4483–4489, 2011.

Cabedo-Sanz, P., Belt, S. T., Jennings, A. E., Andrews, J. T., and Geirsdóttir, Á.: Variability in drift ice export from the Arctic Ocean to the North Icelandic Shelf over the last 8000 years: a multi-proxy evaluation, Quaternary Science Reviews, 146, 99–115, 2016.

Chance, K.: Analysis of BrO measurements from the global ozone monitoring experiment, Geophysical Research Letters, 25, 3335–3338, 1998.

Cuevas, C. A., Maffezzoli, N., Corella, J. P., Spolaor, A., Vallelonga, P., Kjær, H. A., Simonsen, M., Winstrup, M., Vinther, B., Horvat, C., et al.: Rapid increase in atmospheric iodine levels in the North Atlantic since the mid-20th century, Nature communications, 9, 1452, 2018.

Dokken, T. M. and Jansen, E.: Rapid changes in the mechanism of ocean convection during the last glacial period, Nature, 401, 458–461, 1999.

Draxler, R. and Hess, G.: Description of the HYSPLIT 4 modeling system NOAA Tech, NOAA Tech Memo ERL ARL-224, 24, 1997.

Draxler, R. R. and Hess, G.: An overview of the HYSPLIT_4 modelling system for trajectories, Australian meteorological magazine, 47, 295–308, 1998.

Draxler, R. R., Stunder, B., Rolph, G., and Taylor, A.: HYSPLIT4 Users's Guide, US Department of Commerce, National Oceanic and Atmospheric Administration, Environmental Research Laboratories, Air Resources Laboratory, 1999.

Hansson, M. E.: The Renland ice core. A Northern Hemisphere record of aerosol composition over 120,000 years, Tellus B, 46, 390–418, https://doi.org/10.1034/j.1600-0889.1994.t01-4-00005.x, http://dx.doi.org/10.1034/j.1600-0889.1994.t01-4-00005.x, 1994.

Hoff, U., Rasmussen, T. L., Stein, R., Ezat, M. M., and Fahl, K.: Sea ice and millennial-scale climate variability in the Nordic seas 90 [thinsp] kyr ago to present, Nature Communications, 7, 2016.

Kalnay, E., Kanamitsu, M., Kistler, R., Collins, W., Deaven, D., Gandin, L., Iredell, M., Saha, S., White, G., Woollen, J., et al.: The NCEP/NCAR 40-year reanalysis project, Bulletin of the American meteorological Society, 77, 437–471, 1996.

Kaufmann, P. R., Federer, U., Hutterli, M. A., Bigler, M., Schüpbach, S., Ruth, U., Schmitt, J., and Stocker, T. F.: An improved continuous flow analysis system for high-resolution field measurements on ice cores, Environmental science & technology, 42, 8044–8050, 2008.

Kindler, P., Guillevic, M., Baumgartner, M., Schwander, J., Landais, A., and Leuenberger, M.: Temperature reconstruction from 10 to 120 kyr b2k from the NGRIP ice core, Climate of the Past, 10, 887–902, 2014.

Kreher, K., Johnston, P., Wood, S., Nardi, B., and Platt, U.: Ground-based measurements of tropospheric and stratospheric BrO at Arrival Heights, Antarctica, Geophysical Research Letters, 24, 3021–3024, 1997.

Legrand, M. R. and Delmas, R. J.: Formation of HCl in the Antarctic atmosphere, Journal of Geophysical Research: Atmospheres, 93, 7153–7168, 1988.

Lewis, E. R. and Schwartz, S. E.: Sea salt aerosol production: mechanisms, methods, measurements, and models-A critical review, vol. 152, American Geophysical Union, 2004.

McManus, J. F., Francois, R., Gherardi, J.-M., Keigwin, L. D., and Brown-Leger, S.: Collapse and rapid resumption of Atlantic meridional circulation linked to deglacial climate changes, Nature, 428, 834, 2004.

Millero, F. J., Feistel, R., Wright, D. G., and McDougall, T. J.: The composition of Standard Seawater and the definition of the Reference-Composition Salinity Scale, Deep Sea Research Part I: Oceanographic Research Papers, 55, 50–72, https://doi.org/10.1016/j.dsr.2007.10.001, 2008.

Müller, J. and Stein, R.: High-resolution record of late glacial and deglacial sea ice changes in Fram Strait corroborates ice–ocean interactions during abrupt climate shifts, Earth and Planetary Science Letters, 403, 446–455, 2014.

Müller, J., Wagner, A., Fahl, K., Stein, R., Prange, M., and Lohmann, G.: Towards quantitative sea ice reconstructions in the northern North Atlantic: a combined biomarker and numerical modelling approach, Earth and Planetary Science Letters, 306, 137–148, 2011.

Pratt, K. A., Custard, K. D., Shepson, P. B., Douglas, T. A., Pöhler, D., General, S., Zielcke, J., Simpson, W. R., Platt, U., Tanner, D. J., et al.: Photochemical production of molecular bromine in Arctic surface snowpacks, Nature Geoscience, 6, 351–356, 2013.

Rasmussen, T. L., Thomsen, E., and Moros, M.: North Atlantic warming during Dansgaard-Oeschger events synchronous with Antarctic warming and out-of-phase with Greenland climate, Scientific reports, 6, 20 535, 2016.

Richter, A., Wittrock, F., Eisinger, M., and Burrows, J. P.: GOME observations of tropospheric BrO in northern hemispheric spring and summer 1997, Geophysical Research Letters, 25, 2683–2686, 1998.

Saiz-Lopez, A. and von Glasow, R.: Reactive halogen chemistry in the troposphere, Chemical Society Reviews, 41, 6448–6472, 2012.

Spolaor, A., Vallelonga, P., Gabrieli, J., Martma, T., Björkman, M., Isaksson, E., Cozzi, G., Turetta, C., Kjær, H., Curran, M., et al.: Seasonality of halogen deposition in polar snow and ice, Atmospheric Chemistry and Physics, 14, 9613–9622, 2014.

Spolaor, A., Vallelonga, P., Turetta, C., Maffezzoli, N., Cozzi, G., Gabrieli, J., Barbante, C., Goto-Azuma, K., Saiz-Lopez, A., Cuevas, C. A., and Dahl-Jensen, D.: Canadian Arctic sea ice reconstructed from bromine in the Greenland NEEM ice core, Scientific Reports, 6, 33 925, 2016.

Stein, A., Draxler, R. R., Rolph, G. D., Stunder, B. J., Cohen, M., and Ngan, F.: NOAA's HYSPLIT atmospheric transport and dispersion modeling system, Bulletin of the American Meteorological Society, 96, 2059–2077, 2015.

Tzedakis, P., Crucifix, M., Mitsui, T., and Wolff, E. W.: A simple rule to determine which insolation cycles lead to interglacials, Nature, 542, 427, 2017.

Vallelonga, P., Maffezzoli, N., Moy, A. D., Curran, M. A., Vance, T. R., Edwards, R., Hughes, G., Barker, E., Spreen, G., Saiz-Lopez, A., et al.: Sea-ice-related halogen enrichment at Law Dome, coastal East Antarctica, Climate of the Past, 13, 171, 2017.

Vinther, B. M., Clausen, H. B., Johnsen, S. J., Rasmussen, S. O., Andersen, K. K., Buchardt, S. L., Dahl-Jensen, D., Seierstad, I. K., Siggaard-Andersen, M.-L., Steffensen, J. P., et al.: A synchronized dating of three Greenland ice cores throughout the Holocene, Journal of Geophysical Research: Atmospheres, 111, 2006.

Vogt, R., Crutzen, P. J., and Sander, R.: A mechanism for halogen release from sea-salt aerosol in the remote marine boundary layer, Nature, 383, 327–330, 1996.

Wagner, T. and Platt, U.: Satellite mapping of enhanced BrO concentrations in the troposphere, Nature, 395, 486, 1998.

Winstrup, M., Svensson, A. M., Rasmussen, S. O., Winther, O., Steig, E. J., and Axelrod, A. E.: An automated approach for annual layer counting in ice cores, Climate of the Past, 8, 1881–1895, https://doi.org/10.5194/cp-8-1881-2012, http://www.clim-past.net/8/1881/2012/, 2012.

Xiao, X., Zhao, M., Knudsen, K. L., Sha, L., Eiríksson, J., Gudmundsdóttir, E., Jiang, H., and Guo, Z.: Deglacial and Holocene sea–ice variability north of Iceland and response to ocean circulation changes, Earth and Planetary Science Letters, 472, 14–24, 2017.

Yang, X., Pyle, J. A., and Cox, R. A.: Sea salt aerosol production and bromine release: Role of snow on sea ice, Geophysical Research Letters, 35, 2008.

Yang, X., Pyle, J., Cox, R., Theys, N., and Roozendael, M. V.: Snow-sourced bromine and its implications for polar tropospheric ozone, Atmospheric Chemistry and Physics, 10, 7763–7773, 2010.

Zhao, X., Strong, K., Adams, C., Schofield, R., Yang, X., Richter, A., Friess, U., Blechschmidt, A.-M., and Koo, J.-H.: A case study of a transported bromine explosion event in the Canadian high arctic, Journal of Geophysical Research: Atmospheres, 121, 457–477, 2016.

Clim. Past Discuss., https://doi.org/10.5194/cp-2018-80
Manuscript under review for journal Clim. Past
Discussion started: 17 July 2018

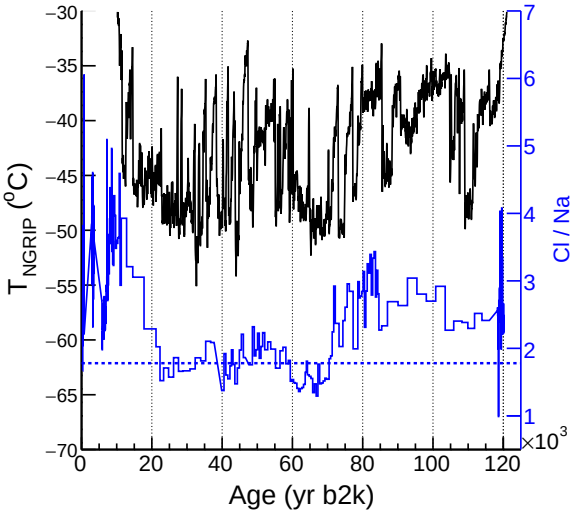

Figure 1. Cl/Na mass ratio time series used for the calculation of ssNa. NGRIP (central Greenland) temperature reconstruction (black, Kindler et al. 2014). Renland Cl/Na mass ratio time series (blue). The sea water reference value (1.8) is indicated by the dotted line. A sodium crustal correction was applied only for ice samples with Cl/Na < 1.8. See Fig. B1 for the RECAP and NGRIP core locations. 'yr b2k' = years before AD 2000.

Clim. Past Discuss., https://doi.org/10.5194/cp-2018-80
Manuscript under review for journal Clim. Past
Discussion started: 17 July 2018

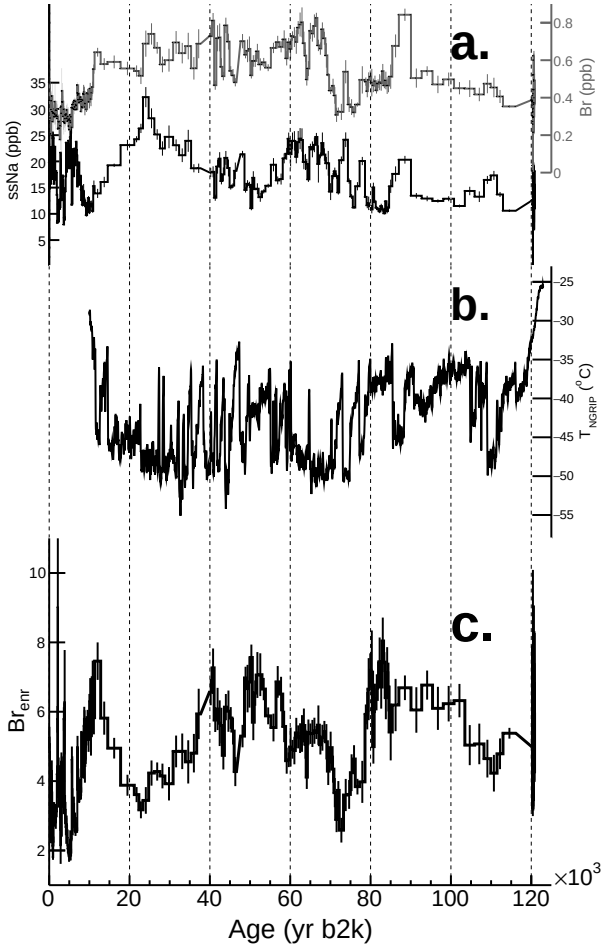

Figure 2. 120 kyr record of sodium and bromine in the RECAP ice core. (a) Concentrations of bromine (Br, grey) and sea-salt sodium (ssNa, black). The last 8 kyr are 100 year averages. The experimental uncertainties (1σ) are indicated. (b) NGRIP temperature reconstruction (Kindler et al., 2014). (c) Bromine enrichment, $\mathrm{Br_{enr}}$ (calculated with Eq. 1-2-3). The error bars are propagated from the experimental bromine and sodium uncertainties.

Clim. Past Discuss., https://doi.org/10.5194/cp-2018-80
Manuscript under review for journal Clim. Past
Discussion started: 17 July 2018

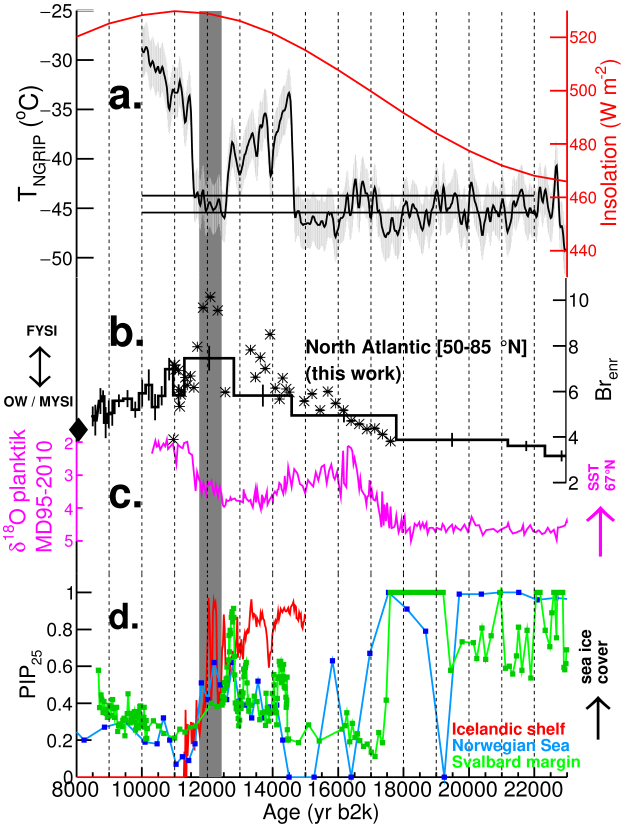

Figure 3. Climate records during the last deglaciation. (a) The black line is the NGRIP temperature reconstruction (Kindler et al., 2014). The light grey band corresponds to single temperature uncertainties (1σ = 2.5 °C). The two horizontal lines correspond to a $\pm 2\sigma$ deviation from the mean temperature (-44.6 °C) found during the 12.4-11.8 kyr period of maximum $\mathrm{Br_{enr}}$ (dark grey band). The red line is the 21 June daily mean insolation at 65 °N (Tzedakis et al., 2017). (b) RECAP $\mathrm{Br_{enr}}$ (thick black line) and repeat sampling conducted at higher resolution (stars). Greater $\mathrm{Br_{enr}}$ values indicate more extensive FYSI. The average $\mathrm{Br_{enr}}$ value measured during the Holocene is indicated by a diamond. (c) Planktonic $\delta^{18}\mathrm{O}$ record (expressed in permil) from sediment core MD95-2010 (66° 41.05' N; 04° 33.97' E, from Dokken and Jansen 1999). Lower $\delta^{18}\mathrm{O}$ values indicate warmer and fresher ocean waters. (d) $\mathrm{P_DIP_{25}}$ records from the Norwegian Sea (blue, core JM11-FI-19PC, Hoff et al. 2016), the Svalbard margin (green, core MSM5/5-712-2, Müller and Stein 2014) and $\mathrm{P_BIP_{25}}$ from the North Icelandic shelf (red, core MD99-2272, Xiao et al. 2017). The $\mathrm{PIP_{25}}$ scale varies from perennial sea ice ($\mathrm{PIP_{25}} \approx 1$) to open water ($\mathrm{PIP_{25}} \approx 0$) conditions (see Fig. 4). All time series are plotted on their original chronologies. See Fig. B1 for core locations.

Clim. Past Discuss., https://doi.org/10.5194/cp-2018-80
Manuscript under review for journal Clim. Past
Discussion started: 17 July 2018

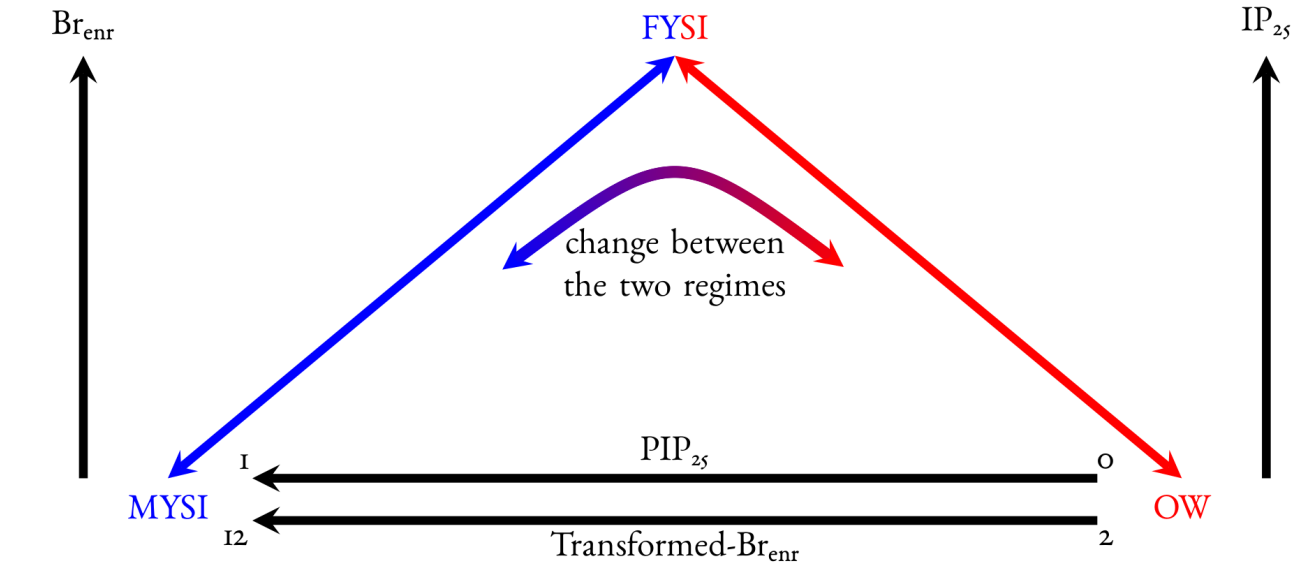

Figure 4. Schematic illustration of marine and ice core-based sea ice indicators as a function of different sea ice conditions. Br_{enr} (ice core) and IP_{25} (sediment core) increase as a function of FYSI area. Low values can thus indicate either open water (OW) or multi-year sea ice (MYSI) conditions, depending on the climate state. The PIP_{25} index is a marine-derived semi-quantitative indicator of local sea ice conditions at the marine core location. $PIP_{25}\sim0$ ($PIP_{25}\sim1$) indicates open water (perennial sea ice, i.e. MYSI) conditions, while intermediate PIP_{25} values reflect seasonal sea ice (i.e. FYSI). The transformed-Br_{enr} reflects an integrated sea ice extent within the RECAP core area of influence (North Atlantic, 50-85 °N). The indicated numbers (2 and 12) are associated with the range of oscillation of the transformed-Br_{enr} variable as a result of the transformation (see also Fig. 5).

Clim. Past Discuss., https://doi.org/10.5194/cp-2018-80
Manuscript under review for journal Clim. Past
Discussion started: 17 July 2018

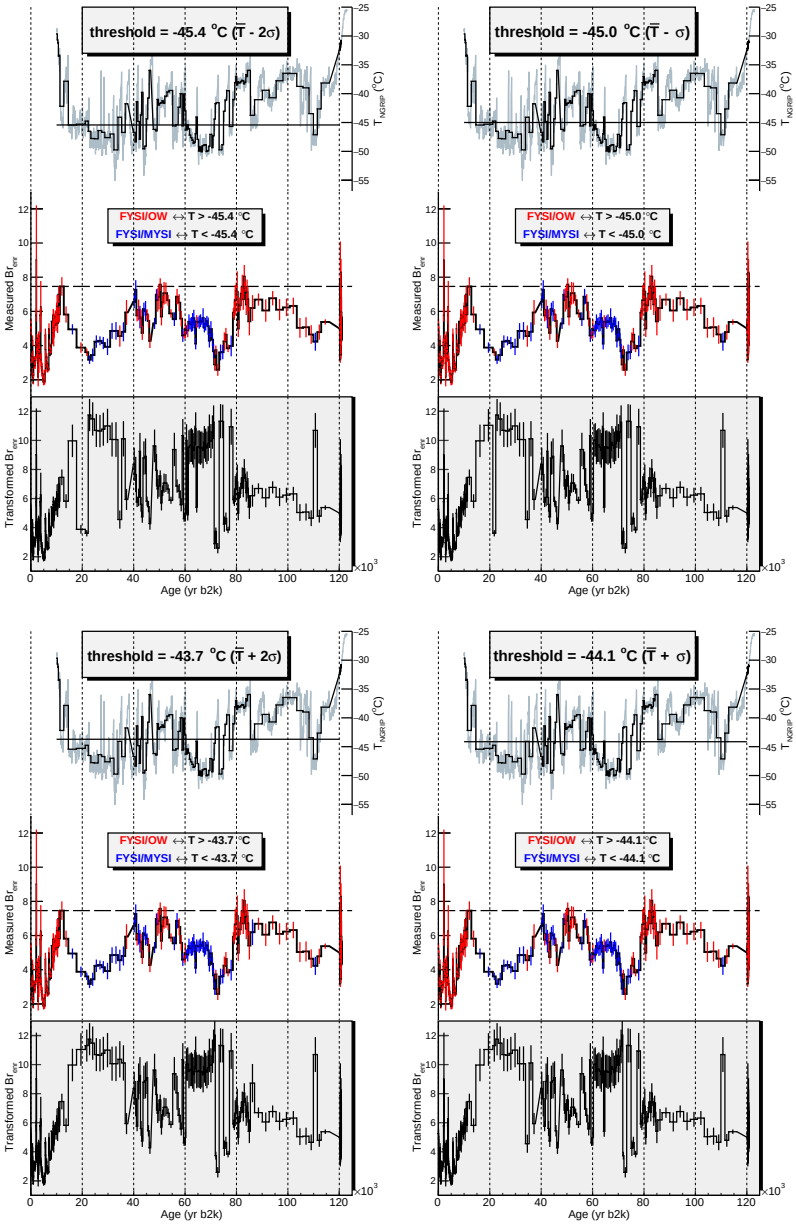

Figure 5. Discrimination of the two $\mathrm{Br_{enr}}$ regimes and $\mathrm{Br_{enr}}$ transformation. Upper panels: reconstructed NGRIP temperature (grey, Kindler et al. 2014). The temperature threshold black line corresponds to the mean temperature (T$\pm 2\sigma$: left; T$\pm 1\sigma$: right) during the 11.8-12.4 kyr period, when the change of $\mathrm{Br_{enr}}$ regime was observed (see Fig. 3). The black time series is the temperature profile downscaled to the measured $\mathrm{Br_{enr}}$ resolution. Middle panels: discrimination of the $\mathrm{Br_{enr}}$ regimes computed according to the integrated temperature value with respect to the threshold. The FYSI/OW (FYSI/MYSI) regime is indicated with red error bars (blue error bars). The $\overline{\mathrm{Br_{enr}}}$=7.4$\pm$0.5 value is indicated with a dotted line. Lower panels: transformation of $\mathrm{Br_{enr}}$ according to Eq. 4 and Eq. 5. The transformed-$\mathrm{Br_{enr}}$ is calculated by reflecting the measured $\mathrm{Br_{enr}}$ values about the $\overline{\mathrm{Br_{enr}}}$=7.4$\pm$0.5 axis, only in the FYSI/MYSI regime (blue error bars). Some discrepancies between the four scenarios are found at 17.3-23.3 kyr (LGM), 33.8-35.3 kyr (GS-7 and GI-7) and 71.3-72.8 kyr (GI-19.2 and GS-20).

Clim. Past Discuss., https://doi.org/10.5194/cp-2018-80
Manuscript under review for journal Clim. Past
Discussion started: 17 July 2018

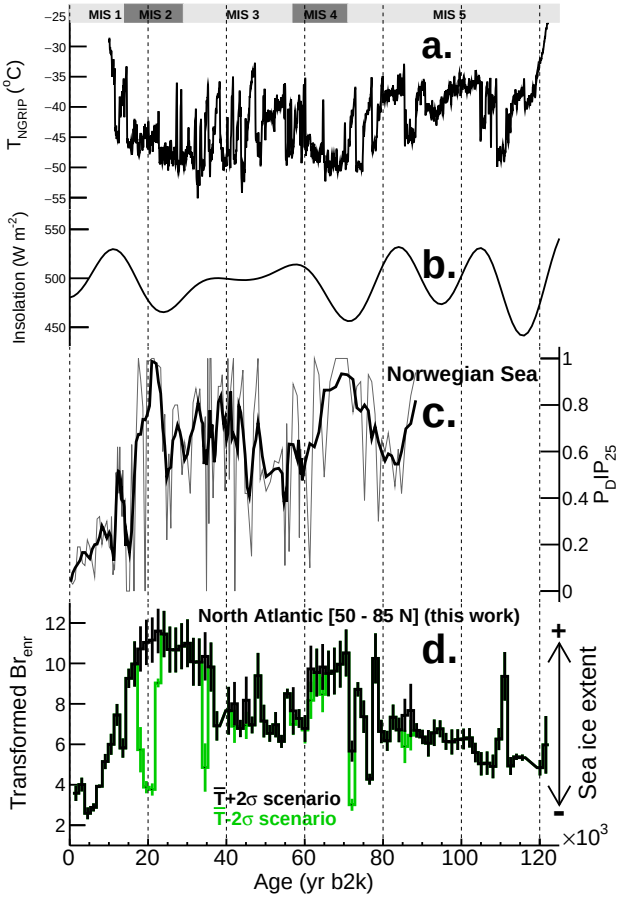

Figure 6. 120 kyr record of sea ice in the North Atlantic. (a) NGRIP temperature reconstruction, from Kindler et al. 2014. (b) 21 June daily mean insolation at 65 °N, from Tzedakis et al. 2017. (c) 90 kyr P_DIP_{25} record from the Norwegian Sea (grey, from Hoff et al. 2016) and 5-point running mean (black). (d) RECAP ice core 1500 year resolution record of transformed-Br_{enr} according to the T+2σ (black) and T-2σ (green) temperature threshold (see Section 3.2, Fig. 5). The T+2σ (black) scenario is more consistent with available evidence of glacial sea ice extent. The only discrepancies between the two T$\pm$2σ reconstructions are at 23.3-17.3 kyr (LGM), 35.3-33.8 kyr (GS-7 and GI-7) and 72.8-71.3 kyr (GI-19.2 and GS-20), where the NGRIP temperatures are close to the threshold.

Clim. Past Discuss., https://doi.org/10.5194/cp-2018-80
Manuscript under review for journal Clim. Past
Discussion started: 17 July 2018

Climate of the Past Discussions

Appendix A: The RECAP ice core samples

The RECAP (REnland ice CAP) ice core was retrieved from the Renland ice cap (71° 18' 18" N; 26° 43' 24" W; 2315 m a.s.l.) from May 13th to June 12th, 2015. The ice cap is located on the Renland peninsula and is independent of the main Greenland ice sheet, with fjords to the north and south. A 98 mm diameter ice core was recovered to 584 m (bedrock). The drilling occurred in a dry borehole to 130 m depth and estisol 140 drilling fluid was used for the remaining depth. The record covers the last 120 kyr. The age-depth model is based on annual layer counting for the interval 0-4 kyr, using the StratiCounter algorithm (Winstrup et al., 2012), tied to fit 25 GICC05-based age markers (Vinther et al., 2006). From 4 to 11.7 kyr, it is created using a shape-preserving piecewise cubic interpolation between 16 GICC05-based markers while from 11.7 to 120.8 kyr the chronology is created by linear interpolation between 74 age markers, the last 3 being estimated from gas-correlation between NGRIP and RECAP $\mathrm{CH_4}$ and $^{18}\mathrm{O}$ air measurements (Simonsen et al., in preparation). The ice core samples (n=1205) were collected and automatically decontaminated from a continuous ice core melting system as part of the RECAP Continuous Flow Analysis (CFA) campaign conducted at the University of Copenhagen in Autumn 2015. The ice core was melted at a speed of approx. 3 $\mathrm{cm\,min^{-1}}$ on a gold coated plate copper melter head (Bigler et al., 2011; Kaufmann et al., 2008). Meltwater was collected continuously from the melter head into pre-cleaned polyethylene vials (cleaned with ultrapure water, > 18.2 $\mathrm{M\Omega cm^{-1}}$) at two different depth resolutions. From the ice cap surface to a depth of 535.15 m, samples incorporated ice meltwater spanning depths of 55 cm. From a depth of 535.15 m to the ice cap bedrock the samples integrated 18.3 cm. The time resolution is annual to multicentennial in the Holocene and from centennial to millennial in the glacial section. After collection, the samples were immediately refrozen at -30 °C and kept in the dark to reduce bromine photolysis reactions. The samples were shipped to Cà Foscari University of Venice (Italy, n=770) and Curtin University of Technology (Perth, Australia, n=435) for determination of bromine ($^{79}\mathrm{Br}$) and sodium ($^{23}\mathrm{Na}$) by Inductively Coupled Plasma - Mass Spectroscopy (CRC-ICP-MS and ICP- SFMS, respectively, see Sect. A1).

A1 Analytical determination of bromine and sodium

A total of 1205 meltwater samples, collected during the Continuous Flow Analysis campaign, were measured in two laboratories. 770 samples were measured in Italy. The depth and age ranges associated with the Italian samples are: surface-150 m (2015 AD-328 yr b2k); 165-219 m (383-636 yr BP); 234-413 m (727-2857 yr b2k); 441-495 m (3522-5749 yr b2k). 435 samples were measured in Australia. The depth and age ranges associated with the Australian samples are: 150-165 m (328-383 yr b2k); 219-234 m (636-727 yr b2k); 413-441 m (2857-3522 yr b2k); 495-562 m (5749-120788 yr b2k).

University Ca' Foscari of Venice, Italy

Bromine and sodium ($^{79}\mathrm{Br}$ and $^{23}\mathrm{Na}$) were determined by Collision Reaction Cell-Inductively Coupled Plasma-Mass Spectrometry (CRC-ICP-MS, Agilent 7500cx, Agilent, California, USA). The introduction system consisted of a ASX-520 autosampler (CETAC Technologies, Omaha, USA) and Scott spray chamber fitted with a MicroFlow PFA nebulizer. The sample flow was kept at 100 $\mathrm{\mu L\,min^{-1}}$. All reagents and standard solutions were prepared with ultrapure water (UPW, 18.2 $\mathrm{M\Omega cm^{-1}}$). Nitric acid (5% v/v, trace metal grade, Romil, Cambridge, UK) and UPW washes (2 minutes each respectively) were used for

background recovery after every sample analysis. The experimental routine (standards and calibrations), as well as the overall instrument performance (detection limits and reproducibility) are the same as in Spolaor et al. 2016.

Curtin University of Technology, Perth, Australia

The analyses were performed by Sector Field Inductively Coupled Plasma Sector Field Mass Spectroscopy in reverse Nier-Johnson geometry (ICP-SFMS, Element XR, Thermo Fisher, Germany) inside a Class 100 clean room environment at Curtin University TRACE facility (Trace Research Advanced Clean Environment Facility). The ICP-SFMS introduction system consisted of an Elemental Scientific Inc. (ESI, Omaha, USA) syringe-pumped autosampler (Seafast II) with a 1 mL PFA capillary injection loop and using an ultrapure water carrier. A 1 ppb indium internal standard in 5% v/v nitric acid ($\mathrm{HNO_3}$, double PFA distilled) flow rate was mixed inline at 25 $\mu\mathrm{L min^{-1}}$ using a T-split (final flow rate of 400 $\mu\mathrm{L min^{-1}}$, take-up time 1.5 min). Nebulization occurred in a peltier cooled (2 $^{\circ}\mathrm{C}$) quartz cyclonic spray chamber (PC3, ESI), fitted with a PFA microconcentric nebulizer (PFA-ST, ESI). Bromine and Na isotope ($^{79}\mathrm{Br}$ and $^{23}\mathrm{Na}$) were detected in medium resolution (10% valley resolution of 4000 amu) and normalized to $^{115}\mathrm{In}$. Memory effects were reduced by rinsing the system between samples with high purity $\mathrm{HNO_3}$ (3%) and UPW. One procedural blank and one quality controlled standard (QC) were analyzed every 5 samples to monitor the system stability. The detection limits for Br and Na were 0.18 ppb and 1.1 ppb respectively (n=80, calculated as 3σ the blank values). The majority of the sample concentrations were above the detection limits for both elements (97%). Control standard concentration relative standard deviations were 9% for Br and 4% for Na (n=82, analyzed over >100 hours). Calibration standards were prepared by sequential dilution (7 standards) of NIST traceable commercial standards (High-Purity Standards, (Charleston, USA)). All materials used for the analytical preparations were systematically cleaned with UPW (18.2>$\mathrm{M\Omega cm^{-1}}$) and double PFA distilled ultrapure $\mathrm{HNO_3}$ (3%, prepared from IQ grade $\mathrm{HNO_3}$, Choice Analytical Pty Ltd, Australia) throughout.

A laboratory intercomparison was performed on a common set of samples (n=140) to investigate differences between the analytical techniques and laboratories, as described in Vallelonga et al. 2017. The correlations and the gradients between the measured concentrations in the two setups are respectively $\rho(\mathrm{Na_{IT}}\text{-}\mathrm{Na_{AUS}})$=0.99 (n=140; p<0.01), $\mathrm{m_{Na}}$= 1.08$\pm$0.01 (1σ) for sodium and $\rho(\mathrm{Br_{IT}}\text{-}\mathrm{Br_{AUS}})$=0.93 (n=140; p<0.01), $\mathrm{m_{Br}}$=1.08$\pm$0.02 (1σ) for bromine.

Appendix B: Sea salt aerosol source area

To infer the sea salt aerosol (SSA) source area for the Renland ice core, daily back trajectories were calculated from 2000 AD to 2016 AD with Hysplit4 (Stein et al., 2015; Draxler et al., 1999; Draxler and Hess, 1998, 1997), using publicly available Reanalysis meteorological data, with a 2.5° resolution in both latitude and longitude (Kalnay et al., 1996). The back trajectories were started daily on an hourly basis at 500 m above the Renland elevation (71.305 °N, 26.723 °W, 2315 m a.s.l.) for the 17 year time span. The trajectory time was set to be 72 hours, representing the average atmospheric lifetime of SSA (Lewis and Schwartz, 2004). To access the potential marine sources of SSA, a selection on the trajectories was implemented, by keeping only those that crossed the marine boundary layer (MBL), defined here as the 900 hPa isosurface (corresponding to approximately 1000 m a.s.l.), for at least 10 hours. This pressure cutoff was chosen according to Lewis and Schwartz 2004 and

Clim. Past Discuss., https://doi.org/10.5194/cp-2018-80
Manuscript under review for journal Clim. Past
Discussion started: 17 July 2018

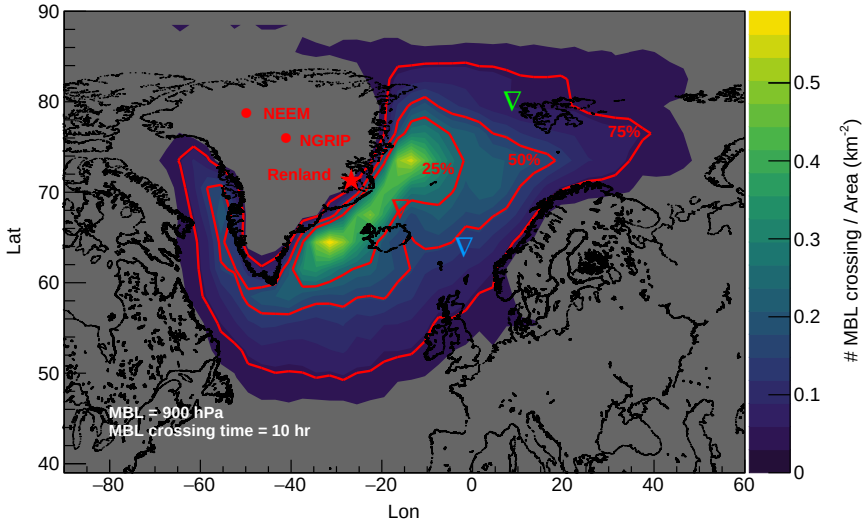

Figure B1. Sea salt aerosol (SSA) source area for the Renland ice core. Spatial distribution of Marine Boundary Layer (MBL) crossings per unit area, derived by applying a 900 hPa constrain for at least 10 hours (see text). The Renland ice cap is marked with a star; the NEEM and NGRIP core sites are marked with a circle. The nablas indicate the marine cores discussed in the text (green: Svalbard margin, Müller and Stein 2014; azure: Norwegian Sea, Hoff et al. 2016; red: North Icelandic shelf, Xiao et al. 2017). The red lines indicate the 75%, 50% and 25% boundaries of the integrated distribution. The 75% contour line is considered to be the SSA source region for the Renland ice core. The source area covers the North Atlantic from ∼50° N to 85° N in latitude. A small SSA contribution is expected from West Greenland waters. Note that areas outside the 75% line with counts <0.05 crossings km^{-2} are not coloured.

references within. The spatial map of the trajectories projected onto the MBL field indicates that 75% of the signal originates from the area spanning from the North Atlantic to the Arctic Ocean (50-85 °N, Fig. B1). A minor contribution is expected from aerosols originated from coastal West Greenland. The consistency of sea ice reconstructions from the Renland ice core and the Nordic Sea sediment cores (see main text) suggests that the Renland source area extends to these regions and this is valid throughout the last 90 kyr. For the overall interpretation of the Renland record the source area is therefore assumed to be the 75% contour region.